IEEE Access
Multidisciplinary ⋮ Rapid Review ⋮ Open Access Journal

Received 25 April 2023, accepted 24 May 2023, date of publication 1 June 2023, date of current version 30 June 2023.

Digital Object Identifier 10.1109/ACCESS.2023.3281365

RESEARCH ARTICLE

A Beam-Steerable Wideband Reflectarray Antenna for C-Band High-Power Microwave Application

LIANG XU, XINGJUN GE, QIANG ZHANG, FANGCHAO DANG, PENG ZHANG, JINLIANG LIU, AND CHENGWEI YUAN

College of Advanced Interdisciplinary Studies, National University of Defense Technology, Changsha 410073, China

Corresponding authors: Xingjun Ge (gexingjun230230@aliyun.com) and Qiang Zhang (119344398@qq.com)

ABSTRACT A beam-steerable wideband reflectarray antenna (WRA) for *C*-band high-power microwave (HPM) application is presented in this paper. The *C*-band WRA comprises a multimode conical horn antenna with high power handling capacity (PHC), 25 × 25 special designed antenna elements, a metal frame and a dielectric plate used as a radome. In our previous work, it has been verified that a wideband prototype using this antenna element has a relative bandwidth of 50% (3.3-5.5 GHz) and its beam scanning range reaches ±60° in low power experiments. In this paper, combined with the equivalent circuit model, the wideband and high PHC property of the WRA element is further explained. To demonstrate the excellent performance of the proposed element in HPM applications, we combined the *C*-band WRA (which was redesigned from the previous wideband prototype) with a well-designed narrowband HPM source operating at 4.3 GHz, and constructed a matching HPM experimental platform. The *C*-band WRA works at 4.1-4.5 GHz, and the results of low power experiments indicate that it can maintain good performance during beam scanning. Its sidelobe level and cross-polarization level are always less than −15 dB and −22 dB, respectively, while its maximum aperture efficiency reached 68.99% (the corresponding antenna gain is 28.07 dB at 4.3 GHz). On the other hand, the PHC of the WRA element reaches 3.82 GW/m^2 and the *C*-band WRA reaches 1.24 GW in simulation. HPM verification experiments have been carried out, and the experimental results show that the PHC of the fabricated prototype exceeded the expectation, which proves that the WRA has broad application prospects in HPM fields.

INDEX TERMS Beam-steerable, wideband reflectarray antenna, high-power microwave (HPM).

I. INTRODUCTION

High power microwave (HPM) technology has broad application prospects such as directed-energy weapon, meteorological radar, microwave energy transmission, biomedicine and plasma heating [1], [2], [3], [4]. In HPM systems, the performance of radiation antenna determines whether the microwave can be effectively radiated, so it is required to have high power handling capacity (PHC) and high efficiency. At present, the commonly used HPM antennas mainly include leaky-wave antennas [5], slotted waveguide array antennas [6], [7], radial line helical array antennas [8], [9] and transmit-array (TA) antennas [10], [11], [12]. Among them, the TA antennas have been widely studied in recent years because of its great beam steering property, but they are usually composed of multilayer TA lens, which is not conducive to the low profile and miniaturization of the radiation system.

Reflectarray antenna (RA), as another implementation of beam-steerable antenna, has attracted the attention of researchers in HPM field. Due to the property of spatial feed, it has the advantages of flexible beam reconfiguration and low profile, which is suitable for HPM applications. There have some HPM RAs based on all-metal helical antenna element [13], dielectric embedded antenna element [14] and

The associate editor coordinating the review of this manuscript and approving it for publication was Sandra Costanzo.

microstrip patch antenna element [15] been reported, but their beam scanning range and PHC need to be further improved. It is worth mentioning that the PHC of the above HPM RAs was obtained by full wave simulation and did not undergo experimental verification. There are still many practical issues that need to be discussed and validated for the application of RAs in HPM conditions. At present, there are almost no practical applications in the publicly reported HPM RAs, except for the Active Denial System (ADS) [16]. However, the mentioned ADS was driven by a 95 GHz, 100 kW continuous wave gyrotron transmitter, and there is currently no experimental research on the low frequency band (*L*-*X* band) and GW level HPM RAs.

We have proposed a wideband reflectarray antenna (WRA) element and its wideband performances are studied in [17], the prototype achieved beam steering within 120° conical region and its relative bandwidth reached 50% (3.3-5.5 GHz). However, its high-power performances have not been verified due to the low PHC of feed antenna and the lack of HPM source. In this paper, the working principle of the WRA element is further explained through an equivalent circuit model. Moreover, combined with a HPM source working at 4.3 GHz, we redesigned a HPM feed antenna, improved the experimental details, designed and built a corresponding HPM experimental platform to verify the performances of the redesigned *C*-band WRA under low power and HPM conditions. As the wideband property of the WRA has been verified, we will mainly discuss the working characteristics of the new prototype in narrowband.

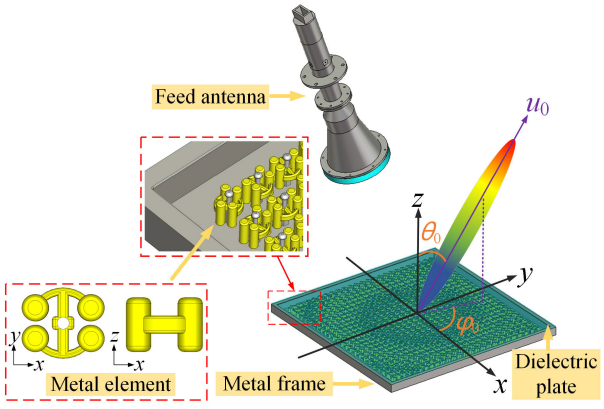

FIGURE 1. Configuration of the C-band WRA.

II. DESIGN OF THE ANTENNA COMPONENTS

Fig.1 shows the configuration of the *C*-band WRA, it consists of a multimode conical horn feed antenna with high PHC, 25 × 25 antenna elements (element spacing is 24 mm, about 0.34 λ_0), a metal frame and a dielectric plate as radome. In this section, the circular polarization (CP) performance, phase shift capability and PHC of the WRA element proposed in [17] were further analysed for the HPM experiment at 4.3 GHz. Moreover, a HPM feed antenna is designed and tested. Subsequently, the design principle of the *C*-band WRA is described.

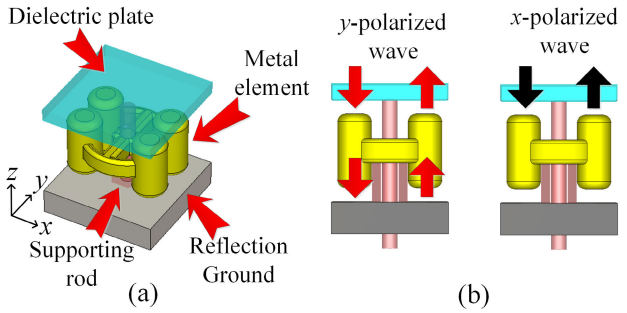

FIGURE 2. Configuration of the WRA element. (a) Structure diagram (b) Schematic diagram of polarization selection characteristic.

A. ANALYSIS OF ANTENNA ELEMENT

The configuration of the WRA element is shown in Fig.2 (a), in [17], we have studied and demonstrated that its relative bandwidth reaches 50% and has high PHC. In this section, we will further explain why it has the above characteristics in conjunction with equivalent circuit models.

Firstly, supported by the dielectric supporting rod, the metal element is suspended on the reflection ground, avoiding electrical connection to the ground and adjacent element, which can effectively reduce mutual coupling between antenna elements. Moreover, the supporting rod plays a role in supporting the dielectric plate, allowing vacuum to be pumped inside the element, thereby improving the PHC of the system. Finally, as depicted in Fig.2 (b), for linear polarization (LP) incident waves, the special designed metal element has the polarization selection characteristic. The LP wave parallel to the centre connecting rod of the metal element is defined as *y*-polarized wave while the LP wave perpendicular to the connecting rod is defined as the *x*-polarized wave. For a circularly polarization (CP) incident wave, it can be divided into two orthogonal LP waves. The *y*-polarized wave can pass through the metal element and be reflected by the reflection ground, while the *x*-polarized wave is directly reflected on the top of the metal element. Thus, the polarization selection characteristic reduces the average power through the metal element to half of the CP incident wave, thereby further improving power capacity. On the other hand, according to the design requirements of Variable Rotation Technique (VRT), when the difference in phase changes between these two LP waves after reflection is π, linear adjustment of the reflection phase can be achieved by rotating the antenna element. This is the core of the beam-steerable property of the *C*-band WRA.

On the other hand, the principles of polarization selection and wideband characteristics can be explained by two simple equivalent circuit models. Firstly, assuming that the four cylinders at the edge of the metal element have the same thickness as the connecting rod (called metal element without cylinders). Removing the metal ground and only considering

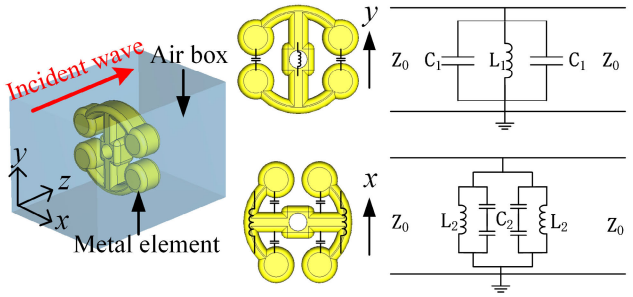

FIGURE 3. Equivalent circuit model of metal element without cylinders.

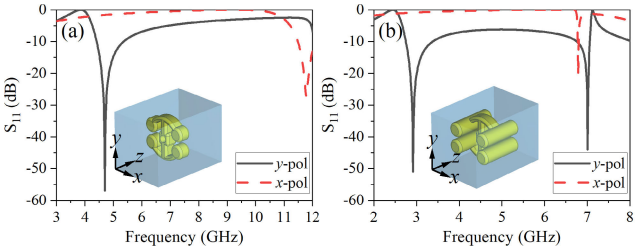

FIGURE 4. Reflection coefficient of metal element in unit cell boundary. (a) Metal element without cylinders (b) metal element with cylinders.

the transmission characteristics of the metal element without cylinders, its equivalent circuit models under y-polarized and x-polarized wave are plotted in Fig.3. Both equivalent circuit models can be simplified as LC parallel resonance circuit with one resonant frequency, the two resonant frequency is about 4.7 and 11.8 GHz as depicted in the S_{11} parameters in Fig.4 (a). As a comparison, the special designed metal element with cylinders has dual-resonance property, the cylinders with a length of approximately $\lambda/2$ introduce a second resonant frequency point, allowing y-polarized wave to pass through the metal elements in a wider frequency band (3-6.5 GHz), while the x-polarized wave is almost reflected as shown in Fig.4 (b).

As mentioned earlier, using VRT to achieve continuous phase adjustment requires a reflection phase difference of π between y-polarized and x-polarized reflected waves, so the available bandwidth of the WRA element (3.5-5.5 GHz in [17]) is smaller than the bandwidth of the polarization selection characteristic of the metal element (3-6.5 GHz).

Under the left-handed circularly polarization (LHCP) incidence, the phase curves of the WRA element at different incident angles (θ) from 0° to 40° is shown in Fig.5, a continuous reflection phase response with 360° phase coverage of the element can be obtained at 4.3 GHz through VRT. With the rotation angle (η) of the metal element changes, the phase shift is approximately twice of the rotation angle as predicted, and the maximum phase difference between the phase curves of $\theta = 0°$ and 40° is about 41°. Combined with the phase synthesis method for HPM RAs proposed in [18], the performance of the C-band WRA can be further improved.

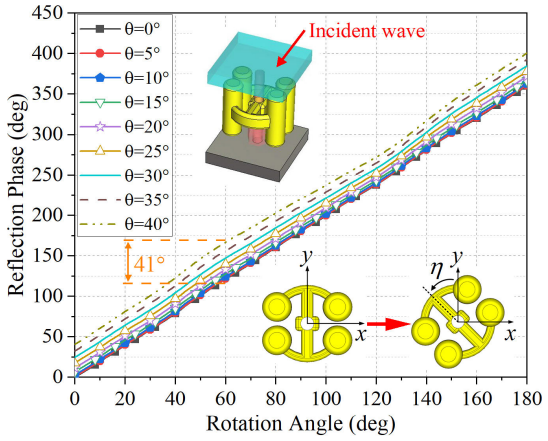

FIGURE 5. Phase curves of the WRA element at 4.3 GHz.

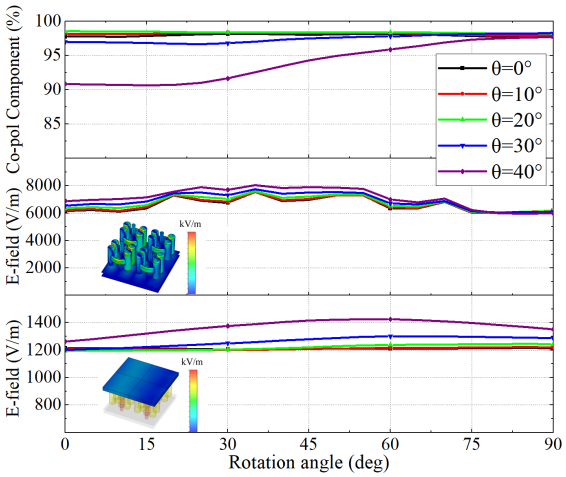

FIGURE 6. Normalized co-polar components and maximum E-field intensity of the WRA element versus rotation angle.

The curves of normalized co-polar components (i.e., LHCP) and maximum electric field (E-field) intensity distribution are shown in Fig.6. Owing to the symmetry of the metal element, the range of its rotation angle only need to be plotted from 0° to 90°. The co-polar components remain above 96% in the range of $\theta = 0°$ to 30°. Even at the large incident angle of 40°, its proportion is always more than 90%. Moreover, when the input power is 0.5 W, the maximum E-field intensities of the metal element and dielectric window (interface of the radome and air) are less than 8100 V/m and 1430 V/m, respectively.

The PHC in HPM application is calculated by [10] and [19]:

$$P_{max} = \left(\frac{E_{break}}{E_{max}}\right)^2 \times P_{in} \tag{1}$$

where E_{break} is the breakdown threshold of E-field, which is usually 50 MV/m for metals in vacuum condition and 3 MV/m in air condition [10], E_{max} is the maximum E-field intensity on the surface and the input power

is P_{in}. Consequently, the PHC of the metal element is $(5 \times 10^7/8100)^2 \times 0.5$ W≈19.05 MW, and the PHC of dielectric window is $(3 \times 10^6/1430)^2 \times 0.5$ W≈2.20 MW. So, the PHC of the WRA element is about 2.20 MW (equivalent to 3.82 GW/m^2).

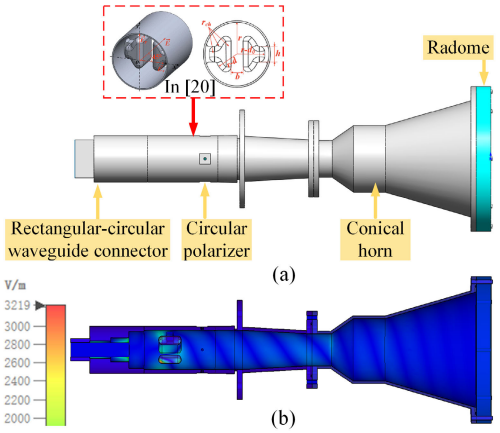

FIGURE 7. Configuration of the feed antenna. (a) Structure diagram (b) E-field distribution.

B. HIGH-POWER MICROWAVE FEED ANTENNA

The designed HPM feed antenna is shown in Fig.7 (a), it composed of a rectangular-circular waveguide connector, a circular polarizer proposed in [20] whose PHC reaches 120 MW, a multimode conical horn, and a radome made of ultra-high molecular weight polyethylene ($\varepsilon_r = 2.3$, $\tan\delta = 0.0003$). Additionally, the simulation result of the E-field distribution inside the feed antenna is displayed in Fig.7 (b), the maximum E-field intensity appears in the circular polarizer. Therefore, the PHC of the feed antenna is $(5 \times 10^7/3219)^2 \times 0.5$ W≈120.63 MW in vacuum condition, consistent with the results in [20].

Conventional power (low power) tests of the feed antenna are carried out in microwave anechoic chamber, the measured results are compared with simulation results in Fig.8. As shown in Fig.8 (a), the measured reflection coefficient is less than −10 dB from 4.1 to 4.5 GHz and it reaches a minimum of −24.9 dB at 4.37 GHz, the difference between measured and simulation results is mainly caused by machining and assembly error. Fig.8 (b) shows that the measured axial ratio is less than 3 dB from 4.15-4.4 GHz, which is basically consistent with simulation. According to Fig.8 (c) and Fig.8 (d), the measured radiation patterns of co-polarization and cross-polarization coincide well with simulation at 4.3 GHz, while the rotational symmetry of the radiation beam is great.

C. DESIGN OF REFLECTARRAY ANTENNA

Using the proposed feed antenna, the C-band WRA which has 25 × 25 antenna elements employed an offset configuration with an f/D ratio of 1.1, and the incident angle of feed antenna is chosen to be 20° (i.e., the height from the phase center of feed antenna to the reflectarray is 660 mm).

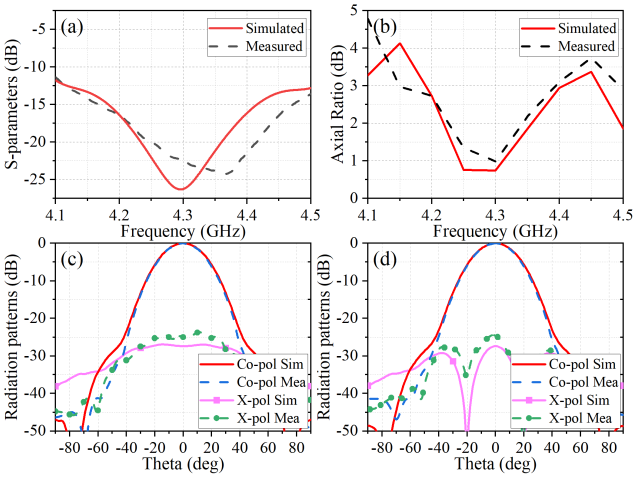

FIGURE 8. Performances of the feed antenna. (a) S-parameters. (b) Axial ratio. (c) Radiation patterns at 4.3 GHz ($\varphi_0 = 0°$) and (d) ($\varphi_0 = 90°$).

Then, the reflection phase required by each element can be calculated by the formulas in [18] and [21]. In [17], it has been demonstrated that the WRA has a beam scanning ability of ±60°, in order to facilitate HPM experiments, we just discuss the C-band WRA within the range of ±40°. Based on the optimization method proposed in [18], the phase distribution for antenna elements of three cases ($\theta_0 = 0°$, 20°, and 40°, $\varphi_0 = 90°$) at 4.3 GHz are calculated and displayed in Fig. 9 (a-c). Moreover, the distribution of incident angle is quantized from 0° to 40° (steps: 5°) as depicted in Fig. 9 (d).

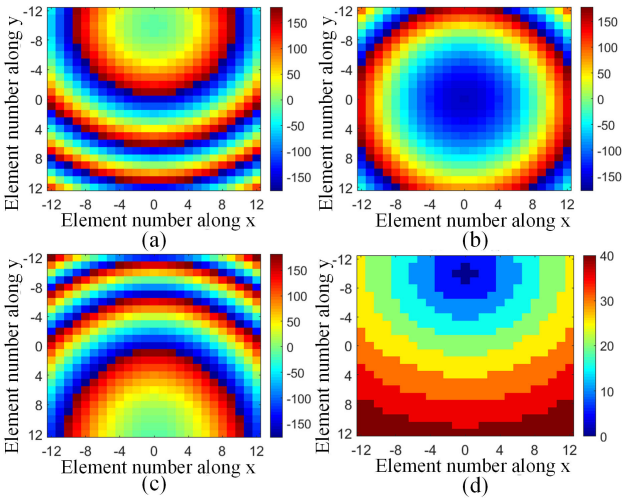

FIGURE 9. Phase distribution of (a) Case 1 ($\theta_0 = 0°$). (b) Case 2 ($\theta_0 = 20°$). (c) Case 3 ($\theta_0 = 40°$) and (d) Quantized incident angle distribution.

On the other hand, in [17], we used protractors to adjust the rotation angle of each metal element, and the error is limited to ±5°. In order to decrease error, we improved the rotation method, the schematic diagram is depicted in Fig.10. Firstly, placing a specially designed positioning plate on the surface of reflectarray, the through-holes on the positioning

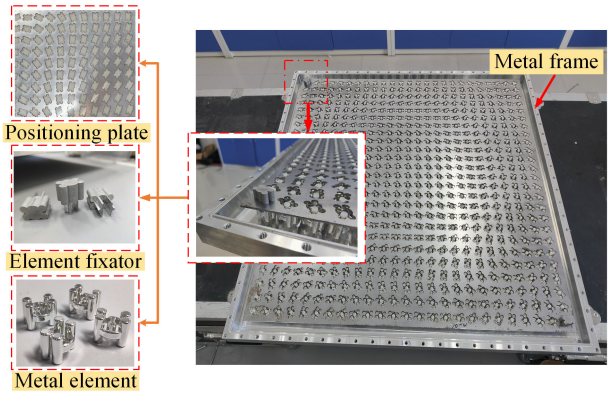

FIGURE 10. Schematic diagram of rotating the metal elements.

plate are processed by laser cutting, and the rotation angle of each through-hole refers to the rotation angle distribution. Then inserting the element fixator into the positioning plate to adjust the rotation angle of the metal element. Finally, removing the positioning plate and covering the metal frame with radome. This method can limit the error of rotation angle within ±0.5°, which makes the experimental results more consistent with the simulation results. Three positioning plates corresponding to Case 1, Case 2 and Case 3 are fabricated for the subsequent experiments.

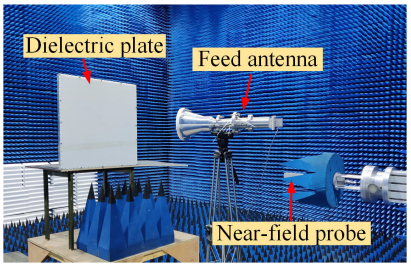

FIGURE 11. Photograph of low power experiments.

III. LOW POWER EXPERIMENTS

Before HPM experiments, the radiation performance of the *C*-band WRA needs to be tested. As shown in Fig.11, the low power experiments are carried out in microwave anechoic chamber. Since the HPM source is operated at 4.3 GHz, Fig.12 compares the simulation and experimental results of radiation patterns at three beam scanning states. The measured results are in good agreement with simulation, and the cross-polarization level is always suppressed below −22 dB. As shown in Table 1, the difference between measured and simulated gain is less than 0.14 dB. During beam scanning, the minimum and maximum axial ratio is 0.35 dB and 1.23 dB, respectively. The experimental results show that the *C*-band WRA has high aperture efficiency and good beam-steerable capability for subsequent HPM experiments.

Moreover, Fig.13 depicts the measured co-polarized radiation patterns at three typical frequency points (4.1, 4.3, 4.5 GHz). It can be seen that the shape of radiation beam is

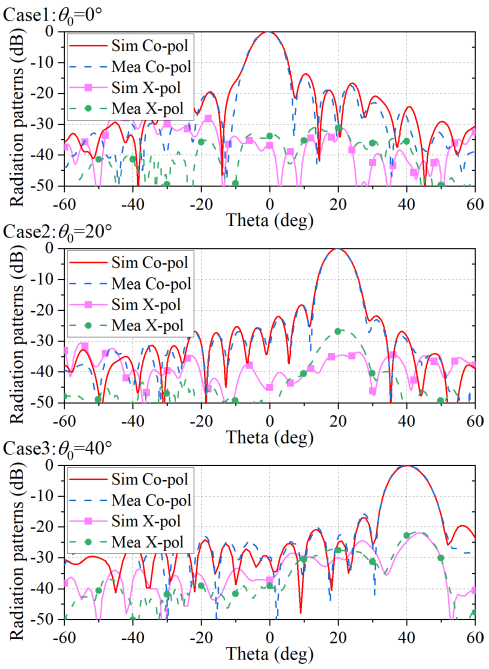

FIGURE 12. Radiation patterns of three beam scanning states at 4.3 GHz.

TABLE 1. Simulated and measured results at 4.3 GHz.

Case	θ_0=0°		θ_0=20°		θ_0=40°	
	Sim	Mea	Sim	Mea	Sim	Mea
Gain (dB)	27.70	27.84	28.11	28.07	27.10	27.06
Sidelobe (dB)	-13.43	-15.10	-18.29	-18.20	-17.13	-16.05
AR (dB)	0.25	0.35	0.31	0.77	1.01	1.23
Aperture efficiency (%)	63.36	65.43	69.63	68.99	55.18	54.68

basically unchanged at three beam scanning states, and their sidelobe levels are always less than −15 dB.

IV. HIGH-POWER MICROWAVE EXPERIMENTS

Firstly, as a comparison of HPM experiments, full wave simulation is used to evaluate the PHC of designed *C*-band WRA. According to the previous analysis, the PHC of the feed antenna is 120 MW due to the limitation of the existing circular polarizer. Thus, the E-field distribution of the prototype is simulated under the conditions of not using the circular polarizer, so that the PHC of the designed array can be more accurately evaluated.

The simulated results are displayed in Fig.14 (a) when the average input power is 1 W. The maximum E-field intensity of 1063 V/m appears on the surface of metal elements, so the PHC of the metal elements under vacuum condition is $(5 \times 10^7/1063)^2 \times 1$ W≈2.21 GW, while the maximum E-field intensity on dielectric window is 85.32 V/m, and its PHC is $(3 \times 10^6/85.32)^2 \times 1$ W≈1.24 GW (equivalent to 3.43 GW/m^2, close to the PHC of WRA element calculated in section II). Due to the PHC of the reflectarray is far exceeding the HPM feed antenna, we fill the reflectarray with

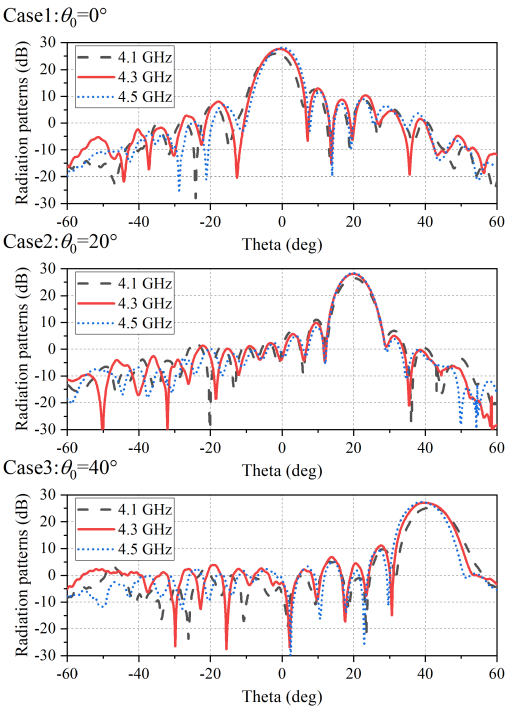

FIGURE 13. Measured radiation patterns of three beam scanning states.

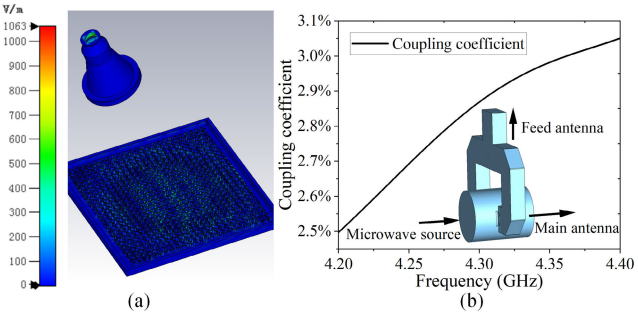

FIGURE 14. (a) E-field distribution of the HPM WRA without circular polarizer. (b) Coupling coefficient of the directional coupler versus frequency.

SF_6 gas instead of vacuuming, the corresponding breakdown threshold can be taken as 9 MV/m. In this way, the PHC of the reflectarray is $(9 \times 10^6/1063)^2 \times 1$ W≈71.68 MW, which is of the same order of magnitude as the HPM feed antenna.

The HPM source in our laboratory is a transit-time oscillator [22], its maximum output power is about 3 GW and the pulse width is about 55 ns at 4.3 GHz now. For HPM experiment, the *C*-band WRA gets tens of megawatts of power from the HPM source by aid of a designed directional coupler. As shown in Fig.14 (b), when a TM_{01} mode microwave output from HPM source, a small part of the energy is coupled and then input into the feed antenna as TE_{10} mode, the rest will be radiated by a main antenna. According to the coupling coefficient curve versus frequency, the input power obtained by the *C*-band WRA is 3 GW × 2.87%≈86.1 MW at 4.3 GHz, which is bigger than the PHC of the reflectarray (71.68 MW), indicating that it can meet the requirement of verifying the PHC of the reflectarray under SF_6 condition.

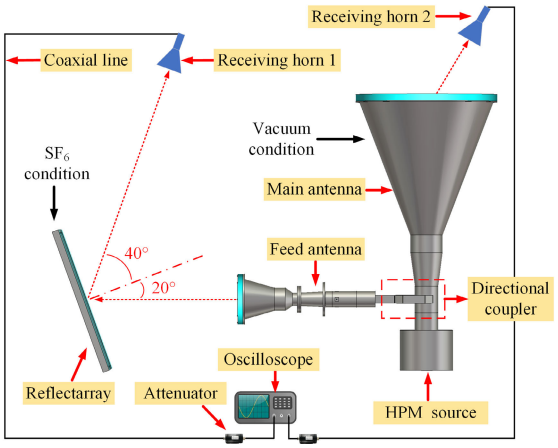

FIGURE 15. Schematic diagram of HPM experiments.

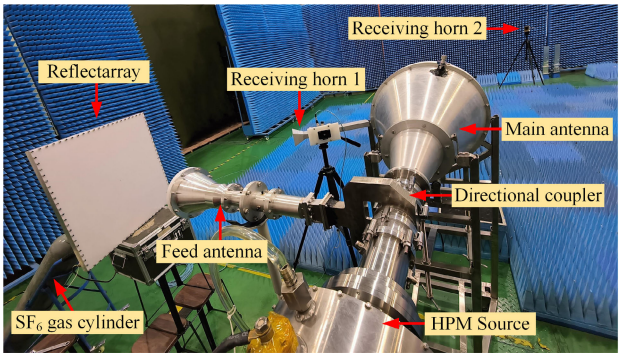

FIGURE 16. Photograph of HPM experiments.

Fig.15 is the schematic diagram of the HPM experiments, two receiving horns are set and connected to the detector via coaxial cables. According to the previous analysis, HPM source, main antenna and feed antenna are operated under vacuum condition, while the reflectarray is filled with SF_6. The photograph of HPM experiments which carried out in microwave anechoic chamber is depicted in Fig.16. By comparing the microwave waveforms detected by the two receiving horns, it can be determined whether breakdown has occurred in the *C*-band WRA. Fig.17 shows the typical results of detected microwaves. According to the figure, there is no grievous breakdown or pulse shortening took place in the experiments, which proves that the PHC of the reflectarray exceeds 86.1 MW under SF_6 condition. This phenomenon also means that if the reflectarray is vacuumized, the PHC of the designed *C*-band WRA is more than 1.24 GW.

Finally, the performances of the *C*-band WRA prototype are compared with representative references as summarized in Table 2, which demonstrated the advantages of WRA in high PHC and wideband HPM applications.

TABLE 2. Comparison of this study and references.

References	Element				Array		
	Antenna type	Element material	Element spacing	Power handling capacity of element	Relative bandwidth	Beam-steering range	Power handling capacity of protype
[11]	Transmit-array	Metal and dielectric	NA	3.5 GW/m^2	0.69 % (14.2-14.3 GHz)	±45°	1 GW (Simulated)
[13]	Reflectarray	All metal	0.65 λ_0	NA	25 % (8.4-10.8 GHz)	±30°	358 MW (Simulated)
[14]	Reflectarray	Metal and dielectric	0.53 λ_0	1 GW/m^2	6 % (9.7-10.3 GHz)	±45°	250 MW (Simulated)
Previous work [17]	Reflectarray	Metal and dielectric	0.35 λ_0 (4.4 GHz)	4.5 GW/m^2	50 % (3.3-5.5 GHz)	±60°	NA
This study			0.34 λ_0 (4.3 GHz)	3.82 GW/m^2	9.3 % (4.1-4.5 GHz)	±40°	1.24 GW (Experimental)

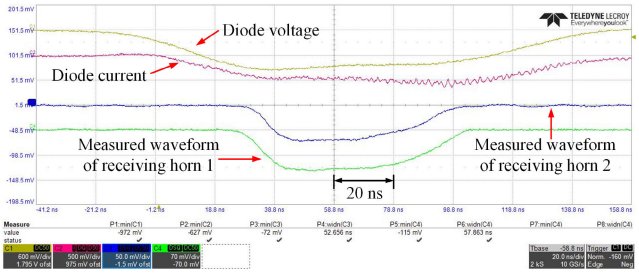

FIGURE 17. Detected microwaves of the main antenna (corresponding to receiving horn 1) and the WRA (corresponding to receiving horn 2).

V. CONCLUSION

In this paper, based on the WRA element proposed in [17], we have further explained the reason of its wideband and high PHC property by equivalent circuit model, and studied its performance under HPM condition. Considering a well-designed HPM source operating at 4.3 GHz, a HPM feed antenna has been designed, the *C*-band WRA is redesigned and the corresponding low power and HPM experimental platform for the prototype are designed and built. The measured results proving that the *C*-band WRA has flexible beam-steerable capability, high aperture efficiency (up to 68.99%), low axial ratio (less than 1.23 dB) and high PHC (1.24 GW, equivalent to 3.43 GW/m^2 in vacuum condition).

It is worth mentioning that combining the design method in this paper, similar experimental results can be obtained by designing any HPM feed antenna in the range of 3.3-5.5 GHz. The reflectarray antenna which using the proposed WRA element has the broad application potential to achieve wideband, high PHC and low profile HPM beam-steerable systems, and this work have important reference value for the design and experimental verification of HPM RAs.

ACKNOWLEDGMENT

(Liang Xu and Xingjun Ge are co-first authors.)

REFERENCES

[1] J. Benford, J. A. Swegle, and E. Schamiloglu, *High Power Microwaves*, 2nd ed. New York, NY, USA: Taylor & Francis, 2007.

[2] R. J. Barker and E. Schamiloglu, *High-Power Microwave Sources and Technologies*. New York, NY, USA: IEEE Press, 2001.

[3] J. Benford, "Space applications of high-power microwaves," *IEEE Trans. Plasma Sci.*, vol. 36, no. 3, pp. 569–581, Jun. 2008, doi: 10.1109/TPS.2008.923760.

[4] Y. Han, G. S. Nusinovich, and T. M. Antonsen, "Effect of electron emission on microparticle heating and melting in high-power microwave systems," *IEEE Trans. Plasma Sci.*, vol. 41, no. 1, pp. 70–76, Jan. 2013, doi: 10.1109/TPS.2012.2225113.

[5] Y. Yang, C. Yuan, and B. Qian, "A beam steering antenna for X-band high power applications," *AEU-Int. J. Electron. Commun.*, vol. 68, no. 8, pp. 763–766, Aug. 2014, doi: 10.1016/j.aeue.2014.03.002.

[6] C.-W. Yuan, S.-R. Peng, T. Shu, Z.-Q. Li, and H. Wang, "Designs and experiments of a novel radial line slot antenna for high-power microwave application," *IEEE Trans. Antennas Propag.*, vol. 61, no. 10, pp. 4940–4946, Oct. 2013, doi: 10.1109/TAP.2013.2273214.

[7] M. N. Y. Koli, M. U. Afzal, and K. P. Esselle, "Significant bandwidth enhancement of radial-line slot array antennas using a radially nonuniform TEM waveguide," *IEEE Trans. Antennas Propag.*, vol. 69, no. 6, pp. 3193–3203, Jun. 2021, doi: 10.1109/TAP.2020.3037689.

[8] X.-Q. Li, Q.-X. Liu, J.-Q. Zhang, and L. Zhao, "16-element single-layer rectangular radial line helical array antenna for high-power applications," *IEEE Antennas Wireless Propag. Lett.*, vol. 9, pp. 708–711, 2010, doi: 10.1109/LAWP.2010.2059371.

[9] Y. Liang, J. Zhang, Q. Liu, and X. Li, "High-power radial-line helical subarray for high-frequency applications," *IEEE Trans. Antennas Propag.*, vol. 66, no. 8, pp. 4034–4041, Aug. 2018, doi: 10.1109/TAP.2018.2840840.

[10] X. Zhao, C. Yuan, L. Liu, S. Peng, Q. Zhang, L. Yu, and Y. Sun, "All-metal beam steering lens antenna for high power microwave applications," *IEEE Trans. Antennas Propag.*, vol. 65, no. 12, pp. 7340–7344, Dec. 2017, doi: 10.1109/TAP.2017.2760366.

[11] Y. Sun, F. Dang, C. Yuan, J. He, Q. Zhang, and X. Zhao, "A beam-steerable lens antenna for Ku-band high-power microwave applications," *IEEE Trans. Antennas Propag.*, vol. 68, no. 11, pp. 7580–7583, Nov. 2020, doi: 10.1109/TAP.2020.2979282.

[12] M. U. Afzal, K. P. Esselle, and M. N. Y. Koli, "A beam-steering solution with highly transmitting hybrid metasurfaces and circularly polarized high-gain radial-line slot array antennas," *IEEE Trans. Antennas Propag.*, vol. 70, no. 1, pp. 365–377, Jan. 2022, doi: 10.1109/TAP.2021.3111522.

[13] G. Kong, X. Li, Q. Wang, and J. Zhang, "A wideband reconfigurable dual-branch helical reflectarray antenna for high-power microwave applications," *IEEE Trans. Antennas Propag.*, vol. 69, no. 2, pp. 825–833, Feb. 2021, doi: 10.1109/TAP.2020.3016379.

[14] X.-H. Zhao, L. Xu, J.-D. Zhang, C.-W. Yuan, Q. Zhang, and Y.-F. Sun, "A dielectric embedded reflectarray for high-power microwave application," *Rev. Sci. Instrum.*, vol. 93, no. 6, Jun. 2022, Art. no. 064703, doi: 10.1063/5.0091106.

[15] G. Kong, X. Li, Q. Wang, and J. Zhang, "A dual-band circularly polarized elliptical patch reflectarray antenna for high-power microwave applications," *IEEE Access*, vol. 9, pp. 74522–74530, 2021, doi: 10.1109/ACCESS.2021.3080823.

[16] K. W. Brown, "Far-field antenna pattern measurement using near-field thermal imaging," *IEEE Trans. Antennas Propag.*, vol. 66, no. 3, pp. 1488–1496, Mar. 2018, doi: 10.1109/TAP.2018.2794351.

[17] L. Xu, C. Yuan, Q. Zhang, J. Liu, Q. Zhang, and Y. Sun, "Design and experiments of a beam-steerable wideband reflectarray antenna for high-power microwave applications," *IEEE Trans. Antennas Propag.*, vol. 71, no. 2, pp. 1955–1959, Feb. 2023, doi: 10.1109/TAP.2022.3232750.
[18] L. Xu, S. Bi, J. Liu, C. Yuan, Q. Zhang, and Y. Sun, "A phase synthesis method for reflectarray in high-power microwave application," *IEEE Trans. Plasma Sci.*, vol. 50, no. 9, pp. 2858–2863, Sep. 2022, doi: 10.1109/TPS.2022.3199430.
[19] X. Zhao, C. Yuan, L. Liu, S. Peng, Z. Bai, and D. Cai, "GW TEM-mode phase shifter for high-power microwave applications," *IEEE Trans. Plasma Sci.*, vol. 44, no. 3, pp. 268–272, Mar. 2016, doi: 10.1109/TPS.2016.2523122.
[20] X. Zhao, C. Yuan, J. Zhang, and Q. Zhang, "Compact circular polarizer based on cross-shaped slot for high-power microwave applications," *Rev. Sci. Instrum.*, vol. 91, no. 1, Jan. 2020, Art. no. 014707, doi: 10.1063/1.5140258.
[21] X. Yang, S. Xu, F. Yang, M. Li, Y. Hou, S. Jiang, and L. Liu, "A broadband high-efficiency reconfigurable reflectarray antenna using mechanically rotational elements," *IEEE Trans. Antennas Propag.*, vol. 65, no. 8, pp. 3959–3966, Aug. 2017, doi: 10.1109/TAP.2017.2708079.
[22] R. Deng, X. Ge, F. Dang, L. Wang, H. Chi, P. Zhang, J. He, and J. Zhang, "Research on a low-magnetic field high-efficiency transit-time oscillator with two bunchers," *IEEE Trans. Plasma Sci.*, vol. 50, no. 3, pp. 656–661, Mar. 2022, doi: 10.1109/TPS.2021.3115939.

LIANG XU was born in Yibin, China, in 1995. He received the B.E. degree in electromagnetic wave propagation and antenna from the University of Electronic Science and Technology of China (UESTC), Chengdu, China, in 2017, and the M.S. degree in physical electronics from the College of Advanced Interdisciplinary Studies, National University of Defense Technology (NUDT), Changsha, in 2019, where he is currently pursuing the Ph.D. degree. His current research interests include antennas and microwave components.

XINGJUN GE was born in Shandong, China, in 1982. He received the Ph.D. degree in physical electronics from the National University of Defense Technology (NUDT), Changsha, China, in 2010.

He is currently an Associate Professor with the College of Advanced Interdisciplinary Studies, NUDT. His current research interests include electron beam devices for high-power microwave (HPM) generation, computational techniques in electromagnetics, and pulse power technology.

QIANG ZHANG was born in Nanyang, Henan, China, in 1984. He received the M.S. and Ph.D. degrees in physical electronics from the National University of Defense Technology (NUDT), Changsha, China, in 2008 and 2012, respectively.

He is currently an Associate Researcher with the College of Advanced Interdisciplinary Studies, NUDT. His current research interests include high-power microwave antenna and microwave components.

FANGCHAO DANG was born in Shaanxi, China, in 1988. He received the Ph.D. degree in physical electronics from the National University of Defense Technology (NUDT), Changsha, China, in 2017.

He is currently an Associate Researcher with the College of Advanced Interdisciplinary Studies, NUDT. His current research interests include high-power microwave (HPM) devices, intense relativistic electron beam (IREB), and microwave radiation systems.

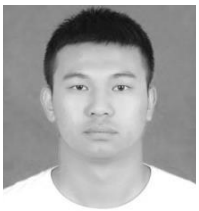

PENG ZHANG was born in Gansu, China, in 1995. He received the B.S. degree in electromagnetic field and wireless technology from the University of Electronic Science and Technology of China (UESTC), Chengdu, China, in 2017. He is currently pursuing the Ph.D. degree with the College of Advanced Interdisciplinary Studies, National University of Defense Technology (NUDT). His current research interest includes vacuum electron devices for high-power microwave (HPM) generation.

JINLIANG LIU was born in Hunan, China, in 1964. He received the B.S. degree from Hunan University, Changsha, China, in 1990, the M.S. degree from the University of Electronic Science and Technology of China, Chengdu, in 1995, and the Ph.D. degree from Tsinghua University, Beijing, China, in 2008.

He is currently with the College of Advanced Interdisciplinary Studies, National University of Defense Technology (NUDT). His current research interests include pulsed-power systems and microwave radiation.

CHENGWEI YUAN was born in Luoyang, Henan, China, in 1974. He received the B.E. degree in applied physics, the M.S. degree in optoelectronics engineering, and the Ph.D. degree in physical electronics from the National University of Defense Technology (NUDT), Changsha, China, in 1997, 2002, and 2006, respectively.

He is currently with the College of Advanced Interdisciplinary Studies, NUDT. His current research interests include antennas and microwave components.